Hypoxia Imaging With PET Correlates With Antitumor Activity of the Hypoxia-Activated Prodrug Evofosfamide (TH-302) in Rodent Glioma Models

Ashley M. Stokes[1,2], Charles P. Hart[3], and C. Chad Quarles[1,2]

[1]Institute of Imaging Science, Department of Radiology and Radiological Sciences, Vanderbilt University, Nashville, Tennessee; [2]Department of Imaging Research, Barrow Neurological Institute, St. Joseph's Hospital and Medical Center, Phoenix, Arizona; and [3]Threshold Pharmaceuticals Inc., South San Francisco, California

Corresponding Author:
C. Chad Quarles, PhD
Department of Imaging Research, Barrow Neurological Institute,
St. Joseph's Hospital and Medical Center, 350 W.
Thomas Road, Phoenix Arizona 85013;
E-mail: Chad.Quarles@BarrowNeuro.org

ABSTRACT

High-grade gliomas are often characterized by hypoxia, which is associated with both poor long-term prognosis and therapy resistance. The adverse role hypoxia plays in treatment resistance and disease progression has led to the development of hypoxia imaging methods and hypoxia-targeted treatments. Here, we determined the tumor hypoxia and vascular perfusion characteristics of 2 rat orthotopic glioma models using 18-fluoromisonidozole positron emission tomography. In addition, we determined tumor response to the hypoxia-activated prodrug evofosfamide (TH-302) in these rat glioma models. C6 tumors exhibited more hypoxia and were less perfused than 9L tumors. On the basis of these differences in their tumor hypoxic burden, treatment with evofosfamide resulted in 4- and 2-fold decreases in tumor growth rates of C6 and 9L tumors, respectively. This work shows that imaging methods sensitive to tumor hypoxia and perfusion are able to predict response to hypoxia-targeted agents. This has implications for improved patient selection, particularly in clinical trials, for treatment with hypoxia-activated cytotoxic prodrugs, such as evofosfamide.

INTRODUCTION

Glioblastoma is the most common type of primary malignant brain tumor. Despite advances in detection and treatment, the prognosis remains poor for patients with glioma with median survival time of only 12–15 months (1). One possible factor contributing to this poor prognosis is hypoxia, as high-grade gliomas can have considerable regions of hypoxia (2-4) with extremely low regional tissue partial pressure of oxygen (pO$_2$) levels of <10 mmHg (4, 5). Hypoxic, but viable, cells can be noninvasively probed with 18-fluoromisonidozole positron emission tomography (^{18}F-FMISO-PET; chemical structure in Figure 1A) (6-8), and the uptake of ^{18}F-FMISO has been found to inversely correlate with overall survival in patients with glioblastoma (7, 9). Using a separate marker for perfusion, Bruehlmeier showed that hypoxia occurs in regions of both hypo- and hyperperfusion (6), suggesting that an independent process leads to a hypoxic phenotype. In addition to hypoxia, ^{18}F-FMISO-PET imaging can also provide a relative measure of perfusion (tracer delivery) using a dynamic scan (6, 10, 11).

Hypoxic tumors are known to have poor response to chemotherapy (12). Insufficient perfusion in hypoxic tumors could reduce the delivery of chemotherapeutic agents and further reduce their effectiveness (13).

Tumor hypoxia is known to lead to both poor long-term prognosis and poor therapeutic response to conventional treatments (3, 14, 15). The adverse role hypoxia plays in treatment resistance and disease progression has led to the development of hypoxia-targeted treatments (16-18). Evofosfamide (also known as TH-302; chemical structure shown in Figure 1B) is a hypoxia-activated prodrug designed to provide significant cytotoxicity in and around extreme hypoxic regions while remaining relatively nontoxic in well-oxygenated regions (19). Using the same hypoxia-targeting moiety as ^{18}F-FMISO, evofosfamide is composed of a hypoxia-sensitive nitroimidazole trigger covalently linked to a cytotoxic bromo-isophosphoramide mustard (18). Evofosfamide is reduced at the nitroimidazole group, leading, under hypoxic conditions, to release of the mustard toxin that acts by alkylating and cross-linking DNA (18-21). Numerous

Figure 1. Chemical structures of 18–fluoromisonidozole (^{18}F-FMISO) (A) and evofosfamide (TH-302) (B).
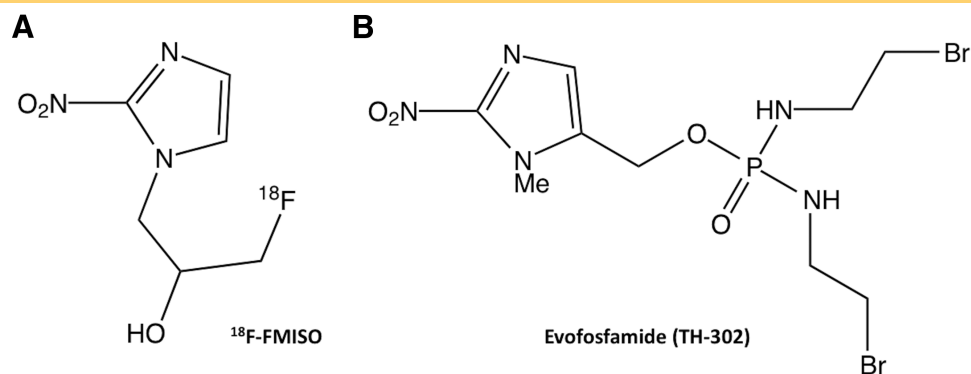
studies have shown broad in vivo activity and efficacy of evofosfamide both as monotherapy or in combination with other chemotherapeutics in preclinical (18, 20-24) and clinical (19, 25, 26) studies.

Because there is substantial heterogeneity in the development and extent of tumor hypoxia, combined with differences in tumor perfusion, ^{18}F-FMISO PET imaging could help select potential patients who would benefit from hypoxia-targeted treatments. Preclinically, 2 commonly used rat glioma models—C6 glioblastomas and 9L gliosarcomas—have markedly different levels of hypoxia and perfusion. In particular, C6 tumors tend to be less vascular and more hypoxic, whereas 9L tumors are more vascular and less hypoxic (27-31). On this basis, C6 tumors, compared with 9L tumors, are expected to be more responsive to evofosfamide. In this study, the perfusion and hypoxia levels in C6 and 9L tumors were determined using ^{18}F-FMISO PET. In addition, C6 and 9L tumor response to evofosfamide treatment was assessed.

MATERIALS AND METHODS

Animals Methods

All animal studies were performed in accordance with National Institutes of Health Institutional Animal Care and Use Committee protocols. For all procedures and imaging, the animals were immobilized in a stereotactic head holder. Anesthesia was induced using 3%–5% isoflurane in air and maintained with 1%–2.5% isoflurane in air. Body temperature was maintained at 38°C using forced warm air. Two rat tumor models were used to provide a range of tumor hypoxia (C6 glioblastomas are relatively hypoxic and 9L gliosarcomas are more normoxic) (29). Male Fischer and Wistar rats (Harlan Laboratories, Indianapolis, Indiana) were inoculated with 1×10^5 9L and C6 glioma cells (American Type Culture Collection, Manassas, Commonwealth of Virginia), respectively, at 1 mm anterior and 3 mm lateral to the bregma, with a depth of 4 mm from the dural surface. Imaging was performed after 14 days. During imaging, the rats were anesthetized with isoflurane in air. The animals were separated into 2 cohorts—one to assess tumor perfusion and hypoxia with ^{18}F-FMISO (cohort 1) and one to assess treatment response to evofosfamide (cohort 2).

Hypoxia Imaging (Cohort 1)

A day before PET imaging, intravenous jugular and arterial catheters were inserted for PET contrast administration and PET blood sampling, respectively. PET data were collected with a microPET Focus 220 system (Concorde Microsystems Inc., Knoxville, Tennessee). Dynamic ^{18}F-FMISO PET (42 time frames/2 h) began simultaneously with bolus injection of ~1.2 mCi (range 1.0–1.4) ^{18}F-FMISO. The reconstructed PET time frames (frames × seconds) were 12 × 10, 8 × 15, 4 × 30, 3 × 60, 3 × 120, 5 × 300, 5 × 600, and 2 × 900 seconds (for a total of 2 hours). To determine the arterial input function, 19 blood samples of 80 μL each were drawn from the arterial catheter into heparinized tubes, with the first 7 blood samples drawn as quickly as possible in the first 90 seconds of PET imaging and the last 12 blood samples drawn at 2, 4, 6, 8, 12, 20, 30, 45, 60, 75, 90, and 120 minutes after injection. Plasma radioactivity was measured using a well counter and then decay-corrected to the time of injection.

Drug Treatment (Cohort 2)

Evofosfamide (Threshold Pharmaceuticals, Inc., South San Francisco, California) dosing solution was prepared immediately before treatment at a concentration of 10 mg/mL in sterile saline. In particular, the evofosfamide solution was vortexed for 1 minute, followed by sonication at 45°C for 30 minutes, and then vortexed every 10 minutes until the solution was clear. This solution was filtered through a 0.2-μm filter before intraperitoneal injection. Following pretreatment imaging, treatment with evofosfamide (50 mg/kg; treated group: C6, n = 8; 9L, n = 6) or sterile saline (control group: C6, n = 8; 9L, n = 6) was performed once daily for 4 days. Post-treatment imaging was performed 1 day after the final treatment (4 days after pretreatment).

Magnetic Resonance Imaging Methods (Cohorts 1 and 2)

Magnetic resonance imaging (MRI) was performed at 4.7 T (Agilent, Santa Clara, California). Anatomical imaging was performed using a T2-weighted fast-spin echo MRI imaging with the following parameters: relaxation time = 2 seconds, echo time = 80 milliseconds, averages = 12, scan time = 3 minutes 16 seconds, field of view = 36 × 36 mm^2, section thickness = 1 mm, and acquisition matrix = 128 × 128 with at least 8 sections (up to 16 sections, as needed). For cohort 1, anatomical images were acquired on the same day as PET imaging. For cohort 2, anatomical images were acquired on the same day as the initial treatment time point (day 0) and 1 day after the final treatment (day 4).

Postprocessing and Analysis (Cohorts 1 and 2)

Image registration was performed using an automated rigid registration algorithm built in-house (Matlab, MathWorks Inc., Natick, Massachusetts), and all registrations were manually verified following registration. For cohort 1, the PET images were initially registered to computed tomography (CT) images, as PET and CT were acquired consecutively using the same animal bed. The CT image was then registered to the magnetic resonance (MR) images (acquired on a separate animal bed), and the resulting transformation matrix was used to register the PET images to the MR images.

The PET data were converted to percentage injected dose per gram of tissue (%ID/g). Perfusion can be determined from the time–activity curves immediately after ^{18}F-FMISO injection. Perfusion was calculating by linear fitting the time–activity curves to obtain the early slope (0–60 seconds) of ^{18}F-FMISO uptake (6, 10). As ^{18}F-FMISO uptake in hypoxic tissues increases over time, a positive late slope (eg, between 1 and 2 hours after injection) can serve as a marker for tumor hypoxia (10, 32, 33). In contrast, normal tissue exhibits decreasing or constant signal at later time points, resulting in zero or negative late slope. The late slope was calculated by linear fitting the time–activity curves from 1 to 2 hours after injection.

As C6 tumors exhibited a wide range of tumor sizes, the effects of tumor size on hypoxia and treatment response were further explored. C6 tumors of cohort 1 were split into groups with tumors sized <25 mm³ (n = 3) and between 25 and 100 mm³ (n = 5). Similarly, C6 tumors of cohort 2 were split into groups with tumors sized <25 mm³ (n = 2), tumors sized between 25 and 100 mm³ (n = 3), and tumors sized >100 mm³ (n = 3). The size distribution of 9L tumors was much smaller.

Statistical Analysis

Data analysis was performed on regions of interest (ROIs) that were initially drawn from anatomical MRI images. For cohort 1, ROIs were drawn in the tumor core and in normal-appearing contralateral rat brain, and these MR-based ROIs were then transferred to the registered PET images for analysis. For cohort 2, tumor ROIs were drawn on the blinded pre- and post-treatment anatomical images. Tumor volume was measured using these MR-based ROIs. Linear tumor growth rates were also calculated from the pre- and post-treatment tumor sizes. Results are presented as means ± standard deviation for rats in each group. Individual groups were statistically compared using paired and unpaired Student t test. Results were considered significant at $P < .05$.

RESULTS

Analysis of Perfusion and Hypoxia in C6 and 9L Tumors

Representative dynamic ^{18}F-FMISO curves are shown in Figure 2 for C6 and 9L tumor models and contralateral normal brain. The perfusion component taken from the first minute following injection was only slightly higher in the C6 tumor compared with that in the contralateral normal tissue, whereas the 9L tumor showed substantially higher perfusion than the normal tissue. At later time points, between 1 and 2 hours after injection, the time–activity curve in C6 tumor ROI steadily increased, whereas the time–activity curves in the 9L tumor and both contralateral normal tissue ROIs remained flat or was decreasing.

The corresponding anatomical MRI, PET perfusion, and PET hypoxia images in Figure 2 show clear differences in perfusion and hypoxia between C6 and 9L tumors (indicated by the arrows). C6 tumors had slightly higher perfusion than the contralateral normal tissue, whereas 9L tumors were characterized by much higher perfusion compared with both C6 tumors and the contralateral normal tissue. The C6 tumor exhibited regions of hypoxia, as identified by a highly positive late slope, whereas 9L tumor appeared normoxic. Two disparate regions in the C6 tumor are evident—one showing higher perfusion and substantial hypoxia (indicated by the arrow) and one showing limited perfusion and hypoxia (indicated by the arrowhead). The 9L tumor exhibited perfusion "hotspots" and hypoxia image contrast consistent with the normal tissue.

C6 and 9L tumor voxels from each rat were combined to determine the regional heterogeneity of perfusion and hypoxia within each tumor type. The boxplots in Figure 3 show the voxelwise perfusion (A) and hypoxia (B) for C6 and 9L tumors (combining all voxels from 8 C6 and 6 9L tumors), respectively. 9L tumors showed a wider range of perfusion values, with higher median perfusion, compared with C6 tumors (0.59 vs 0.36%ID/(g · min)) (Figure 3A). The blue markers indicate the median values for each tumor (C6, n = 8; 9L, n = 6). In addition to a wider voxelwise range for 9L tumors, the median perfusion for each tumor showed greater heterogeneity (C6: median range, 0.29–0.42%ID/(g · min); 9L: 0.33–0.84%ID/(g · min)). Conversely, C6 tumors showed a slightly wider range of hypoxia values (Figure 3B), with both tumor types spanning hypoxic and normoxic late-slope values. For C6 tumors, late slopes between −1.2e-3 and 2.8e-3%ID/(g · min) comprise the 25th to 75th percentile, whereas for the 9L tumor, late slopes between −2.7e-3 and 0.9e-3%ID/(g · min) comprise the 25th to 75th percentile. C6 tumors tend to have higher median hypoxia compared with 9L tumors (0.74e-3 vs −0.96e-3%ID/(g · min)), with most tumors showing positive median late slopes (5 of 8 C6 tumors).

The hypoxia and perfusion values for each rat are shown in the plot in Figure 4A. C6 tumors (black "x", n = 8) exhibited considerably more hypoxia (higher late slope, y-axis) than the contralateral normal tissue (gray "x"), with 6 of the 8 tumors having mean positive late slope values. 9L tumors (black circles, n = 6) had similar late slope values to contralateral normal tissue (gray circles). Perfusion in C6 and 9L tumors was higher than that in the normal tissue. There was no significant correlation between perfusion and hypoxia in either tumor type. Overall, both C6 and 9L tumors had significantly higher perfusion than normal tissue ($P = .0005$ and 0.02, respectively) (Figure 4B). C6 and 9L tumors did not have significantly different perfusion ($P = .07$). The normal tissue perfusion was not significantly different between C6 and 9L groups ($P = .18$). C6 tumors were significantly more hypoxic than the contralateral normal tissue ($P = .0003$) and 9L tumors ($P = .00005$) (Figure 4C). Late slopes in 9L tumors were not significantly different from those in normal tissue
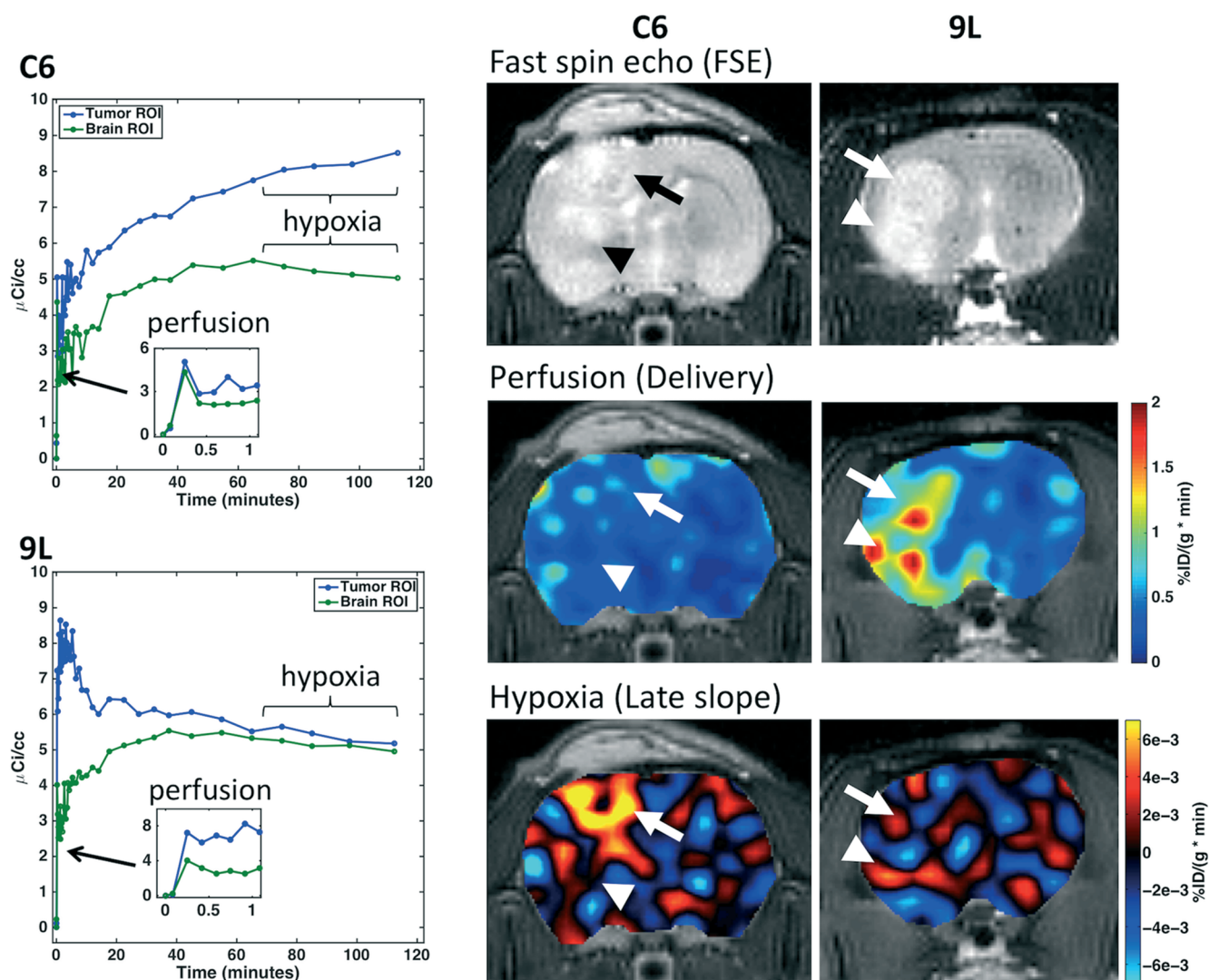
Figure 2. Dynamic 18–fluoromisonidozole positron emission tomography (^{18}F-FMISO PET) time courses in plasma, tumor, and brain regions of interest (ROIs) for rats inoculated with C6 (top left) and 9L (bottom left) tumors. Hypoxia is obtained from the slope of uptake from 1–2 hours after injection. Inset shows first minute of time courses, indicative of perfusion. Example anatomic magnetic resonance imaging (MRI) (top), PET perfusion (middle), and PET hypoxia (bottom) images in C6- and 9L-bearing rats, where the arrows indicate tumor locations.

($P = .3$). The normal tissue late slopes were not significantly different between the groups ($P = .93$).

Determination of Treatment Response to Evofosfamide

Figure 5A shows the pre- and post-treatment tumor volumes for C6 (n = 8) and 9L (n = 6) tumors. The tumor volumes were not significantly different before treatment between the treated and control groups for either tumor type, although C6 tumors had substantially wider range of pretreatment tumor volumes in both the treated (range, 9.0–204 mm³) and control groups (range, 11.5–131.4 mm³). 9L tumors had a much smaller pretreatment size range (8.6–21.7 and 4.6–32.3 for treated and untreated groups, respectively). At the post-treatment time point, the control groups had larger tumors than the treated groups, with significant differences for 9L tumors ($P = .002$).

Because of the wide range of pretreatment tumor sizes in C6 groups, tumor volume was not significant at the post-treatment time point. Post treatment, C6 tumor volumes ranged from 15.9 to 245 mm³ for the treated group and from 38.2 to 328.3 mm³ for the untreated group. 9L post-treatment tumor volumes ranged from 34.6 to 77.5 for the treated group and 82.2 to 141.4 mm³ for the untreated group.

To account for differences in pretreatment tumor size, linear tumor growth rates were calculated for each group (Figure 5B). The mean (± standard deviation) growth rates were 6.5 (±4.2) mm³/d and 25.8 (±16.6) mm³/d for C6 treated and control rats, respectively, and 10.5 (±3.7) mm³/d and 23.1 (±4.7) mm³/d for 9L treated and control rats, respectively. Growth rates in the treated group were significantly smaller than those in the control group ($P = .007$
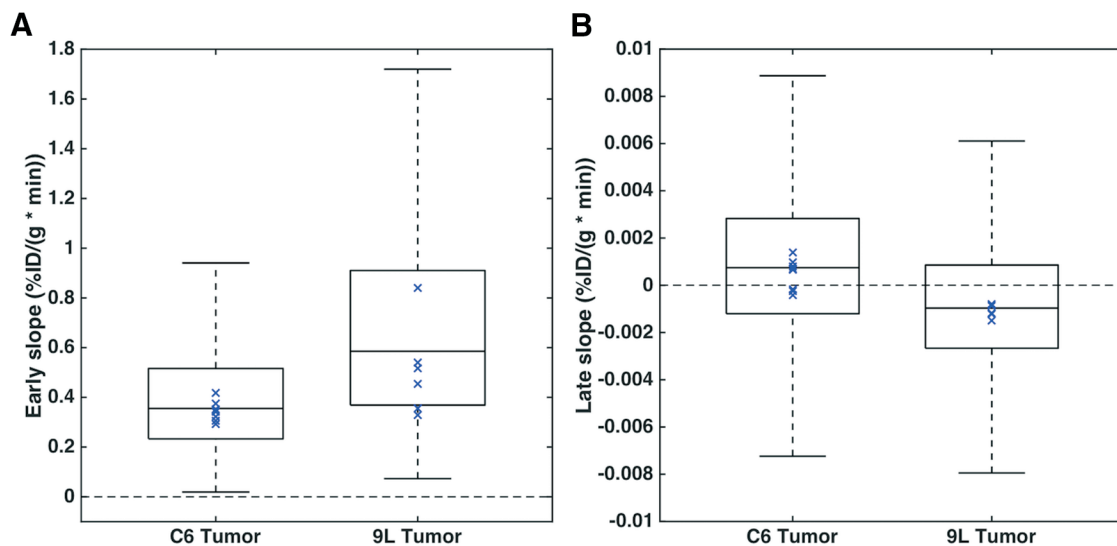
Figure 3. Boxplots showing the voxelwise tumor perfusion (A) and hypoxia (B) for C6 and 9L tumors (voxels from 8 C6 tumors and 6 9L tumors). Blue marker indicates the median values for each tumor (B) (C6, n = 8; 9L, n = 6).

and $P = .0005$ for C6 and 9L, respectively). Accordingly, treatment with evofosfamide resulted in 4- and 2-fold decreases in the tumor growth rates of C6 and 9L tumors, respectively.

As hypoxia levels in C6 tumors are expected to be proportional to the tumor size (27), we further investigated the role of tumor size on both perfusion and hypoxia in cohort 1 and on treatment efficacy in cohort 2. Figure 6A shows that both size groups had significantly different perfusion relative to the normal tissue ($P = .03$ and 0.01 for the <25 mm^3 tumors and $25–100$ mm^3 tumors, respectively), although the level of perfusion did not depend on size ($P = .8$). Both size groups also had significant levels of hypoxia relative to the normal tissue ($P = .04$ and 0.001 for the <25 mm^3 tumors

and $25–100$ mm^3 tumors, respectively) (Figure 6B). In addition, tumors sized $25–100$ mm^3 had showed significantly more hypoxia than tumors sized <25 mm^3 ($P = .0007$). Given the dependence of hypoxia on tumor size, Figure 6C shows the different responses to hypoxia-activated treatment based on initial tumor size. The smallest tumors (<25 mm^3) had slightly smaller tumor growth rates for the treated group compared with those in the control group, but these differences were not statistically significant. Conversely, the larger tumors (>25 mm^3) showed significantly smaller tumor growth rates in the treated group compared with those in the control group ($P = .005$ and 0.04 for the $25–100$ mm^3 and >100 mm^3 groups, respectively).
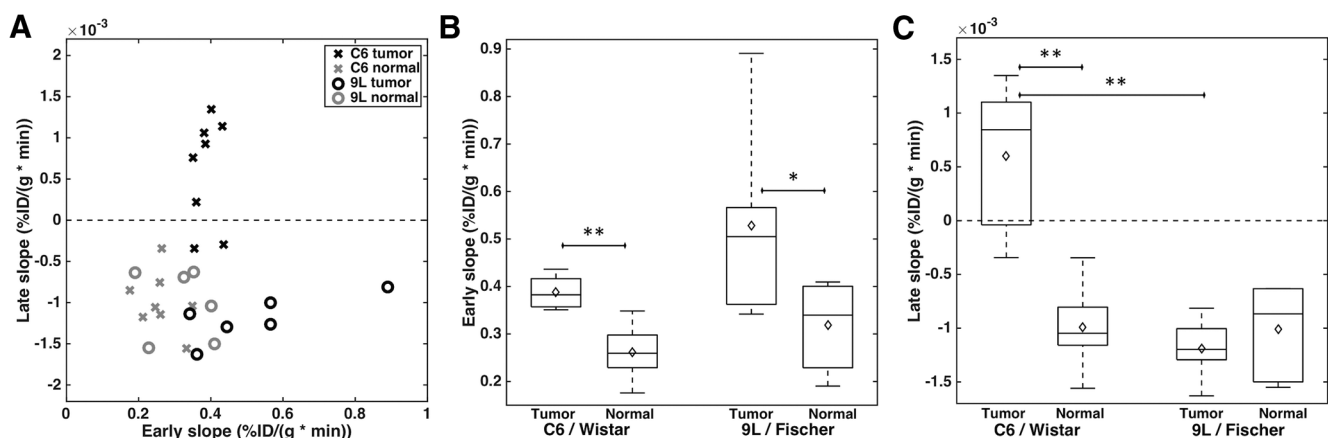
Figure 4. Scatter plot showing mean hypoxia and perfusion for each rat in both tumor and contralateral normal brain (C6 tumor and normal, n = 8; 9L tumor; normal, n = 6) (A). Boxplots for perfusion (B) and hypoxia (C) in C6 and 9L tumors and contralateral normal brain, with diamond markers indicating the mean (B–C). **$P < .01$ and *$P < .05$.
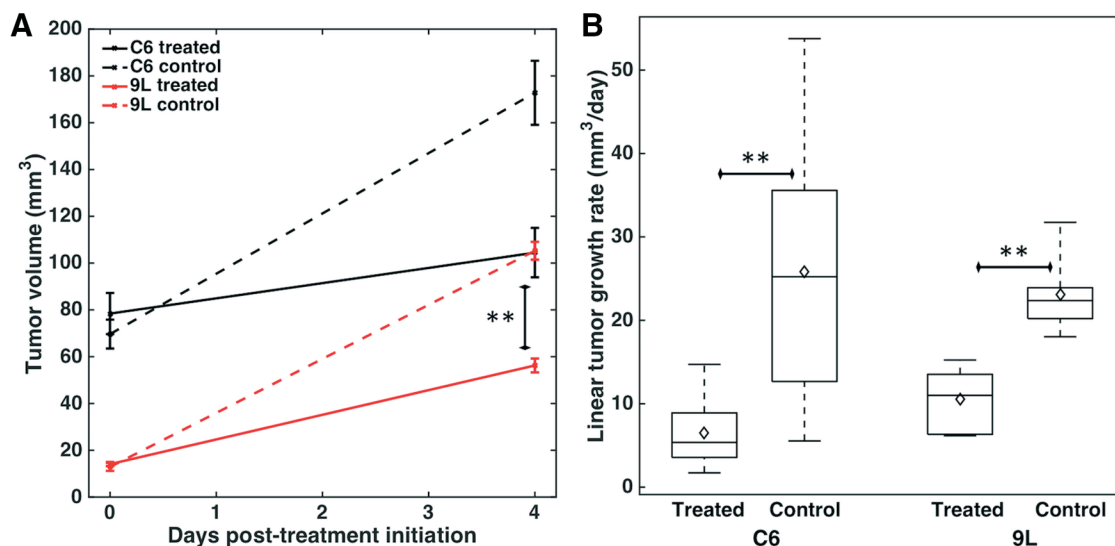
Figure 5. Mean tumor volume pretreatment and 4 days after treatment initiation (mm^3), with error bars indicating standard error of the mean (SEM) (A). Boxplots for linear tumor growth rate (mm^3/d, right) for C6 and 9L treated and control groups (B). **$P < .01$.

DISCUSSION

Hypoxia develops from an imbalance between the supply and consumption of oxygen. Two notable causes of hypoxia are perfusion deficits (acute hypoxia) and oxygen diffusion deficits (chronic hypoxia). Acute hypoxia is associated with abnormal tissue microvasculature and is highly unpredictable. Under chronic hypoxia, tumor cells adapt to the hypoxic microenvironment by upregulating prosurvival proteins; these proteins are associated with increased angiogenesis, proliferation, invasion, and metastases. Although ^{18}F-FMISO could potentially report on either acute or chronic hypoxia (34), it appears likely

that the major source of ^{18}F-FMISO signal results from chronic hypoxia (35). Similarly, evofosfamide could be sensitive to either acute or chronic hypoxia, and recent work has proposed inducing acute hypoxia to improve the efficacy of evofosfamide (36, 37). Another promising alternative would be to combine evofosfamide and a general chemotherapeutic agent to provide more uniform tumor cell death across hypoxic and normoxic tumor regions (22).

Perfusion can have a profound effect on drug efficacy, as access to tumor cells for chemotherapeutic drugs may be limited in the presence of perfusion deficits (13). Previous studies have
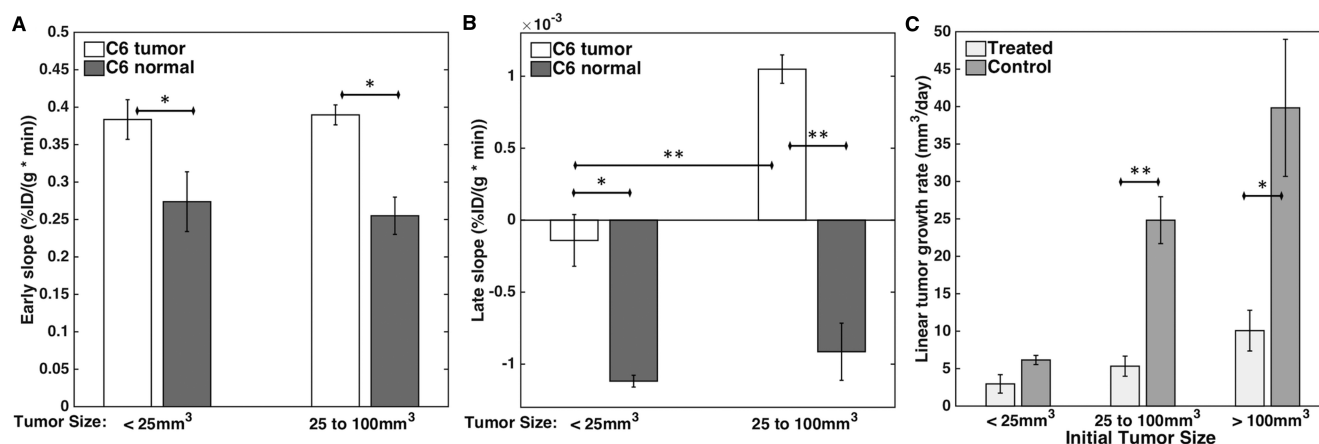
Figure 6. Bar plots showing perfusion (A) and hypoxia (B) in C6 tumors separated by tumor size and the corresponding contralateral normal brain (n = 3 for tumors sized <25 mm^3 and n = 5 for tumors sized between 25 and 100 mm^3). Bar plot showing linear tumor growth rate (mm^3/day) in C6 tumors separated by tumor size for evofosfamide-treated and vehicle-control groups (n = 2 for tumors sized <25 mm^3, n = 3 for tumors sized between 25 and 100 mm^3, and n = 3 for tumors sized >100 mm^3) (C). **$P < .01$ and *$P < .05$.

hypothesized that dynamic PET imaging during the initial bolus injection reports on contrast agent delivery and distribution and is thus related to perfusion (6, 10, 11). In particular, early ^{18}F-FMISO PET images have shown reasonable correlations with ^{15}O-H$_2$O PET (6) and dynamic contrast-enhanced MRI (10) perfusion measurements. The ability to inform on both perfusion and hypoxia within a single scan is clinically advantageous, as combined measurements may be more predictive of outcomes than individual measurements (11). In this study, hypoxia had no significant correlation with perfusion in either tumor type, as observed in other studies (6, 10, 11).

In this study, we used dynamic ^{18}F-FMISO PET to determine perfusion and hypoxia characteristics in C6 and 9L tumors. Although there are alternative hypoxia imaging methods available (eg, other PET tracers, electron paramagnetic resonance, and MRI), (15, 38-40), ^{18}F-FMISO was chosen for this study because it shares the nitroimidazole-targeting moiety with evofosfamide. Dynamic imaging was used so that the temporal characteristics of the tracer flux through the tissue could be leveraged to estimate perfusion and hypoxia. In the case of hypoxia, the use of static images (eg, 1 hour after injection) may be confounded by high tracer delivery, which can yield regions of high PET signal even under normoxic conditions. Pharmacokinetic modeling of the data may provide more quantitative hypoxia and perfusion measures, with moderate additional computational expense. Pharmacokinetic modeling was not performed in this study because of the limited signal-to-noise ratio and input function requirements.

We observed substantial microregional heterogeneity in tumor hypoxia using voxelwise analysis. Both C6 and 9L tumor types exhibited both positive and negative late slopes, although the mean late slope was indicative of hypoxia in only C6 tumors. The higher average ^{18}F-FMISO retention in C6 tumors compared with that in 9L tumors is in good agreement with previous reports using electron paramagnetic resonance (29) and static late ^{18}F-FMISO images (27). In C6 tumors, regional ^{18}F-FMISO heterogeneity was observed using autoradiography and was found to be consistent with the ex vivo pimonidazole staining distribution (41).

Based on previous reports of mean tumor partial pressure of oxygen (pO$_2$) for C6 and 9L tumors (12–14 and 30–32 mmHg, respectively) (29), 9L tumors were expected to respond less to hypoxia-activated treatment with evofosfamide. Despite the lack of overall tumor hypoxia in the ^{18}F-FMISO data, 9L tumors also responded favorably to evofosfamide treatment. Microscopic regions of hypoxia distributed throughout a predominantly normoxic tumor would likely exhibit relatively normal ^{18}F-FMISO uptake overall, particularly given a PET scan's relatively low resolution and partial voluming effects. However, these regions would still be impacted by evofosfamide, which could impact the tumor's growth rate. In addition, 9L tumors in the present study exhibited higher perfusion compared with C6 tumors, which, although not significant, is consistent with higher MRI-based blood volume measurements (27) in 9L tumors. Given the high 9L tumor perfusion, evofosfamide efficacy may be improved by increasing the delivery of the cytotoxic moiety to nearby well-oxygenated cells, under the so-called bystander effect.

One potential drawback in this study was the absence of validation of evofosfamide efficacy using C6 and 9L cultures. Perfusion and hypoxia are not the only modulators of antitumor activity, which also depends on the presence of intracellular reductases needed to activate evofosfamide and the tumor-specific molecular mechanism to effectively repair DNA damage (21, 23). Thus, other contributing factors may have played a role in the observed antitumor activity in this study. Another drawback was the observed size heterogeneity of C6 tumors. To overcome this limitation, C6 tumors were considered as a whole and grouped by size. As hypoxic volume in C6 tumors was previously shown to be proportional to overall tumor volume (27), we investigated whether the severity of hypoxia was influenced by size. The results showed that the severity of hypoxia is dependent on tumor size, whereas that of perfusion is not. In addition, the treatment response in C6 tumors varied with tumor size. Overall, the more hypoxic C6 tumors had a larger response to evofosfamide compared with 9L tumors, as evidenced by the larger reduction in tumor growth rate compared with the control group.

As tumor hypoxia and perfusion are spatially heterogeneous, the treatment response is expected to vary spatially in tumors. In the present study, PET data were acquired in a separate cohort of animals from the treatment cohort (to limit the total amount of time each animal spent under anesthesia). To evaluate local response heterogeneity, on a voxel-by-voxel basis, additional imaging techniques sensitive to tumor cell density (eg, diffusion weighted imaging [DWI]), proliferation (eg, 3′-deoxy-3′-^{18}F-Fluorothymidine), or apoptosis (eg, ^{99m}Tc-Annexin V) could be incorporated into the study. In particular, DWI may be sensitive to early response to cytotoxic drugs, before changes in tumor volume. However, a previous study observed no change in diffusion characteristics with evofosfamide treatment, suggesting that DWI is not sensitive enough to the hypoxic cell fraction changes induced by evofosfamide (23). In contrast, that same study observed a significant change in permeability following evofosfamide treatment, suggesting that an approach that includes a perfusion or permeability component may be a useful biomarker for evofosfamide treatment response. Overall, a multiparametric approach would provide a far more comprehensive assessment of tumor treatment response and may help clinicians better manage subsequent treatment options (eg, surgical planning or stereotactic radiosurgery).

In conclusion, hypoxia is an important factor in the progression of brain tumors and is associated with poor treatment response. Hypoxia can be imaged noninvasively using dynamic ^{18}F-FMISO-PET, with the added benefit of complementary perfusion information. C6 tumors were found to be more hypoxic overall than 9L tumors, whereas 9L tumors exhibited microregional hypoxia and higher overall perfusion than C6 tumors. Evofosfamide is a promising hypoxia-activated prodrug and showed a significant effect on tumor growth rates in the 2 glioma tumor models mentioned in this study. The less hypoxic 9L tumors showed favorable response to evofosfamide, likely because of regional hypoxia and increased perfusion, although the reduction in tumor

growth rates was less than that in the growth rates of C6 tumors. In C6 tumors, both hypoxia characteristics and treatment response were modulated by tumor size, with higher severity of hypoxia and greater treatment response in larger tumors. Evofosfamide is expected to predominantly affect hypoxic tumor regions—which likely vary spatially—highlighting the need for spatially sensitive measures of hypoxia and treatment response.

REFERENCES

1. Stupp R, Hegi ME, Gilbert MR, Chakravarti A. Chemoradiotherapy in malignant glioma: standard of care and future directions. J Clin Oncol. 2007;25(26):4127–4136.
2. Kaur B, Khwaja FW, Severson EA, Matheny SL, Brat DJ, van Meir EG. Hypoxia and the hypoxia-inducible-factor pathway in glioma growth and angiogenesis. Neuro Oncol. 2005;7(2):134–153.
3. Evans SM, Jenkins KW, Chen HI, Jenkins WT, Judy KD, Hwang W-T, Lustig RA, Judkins AR, Gradyt MS, Hahn SM, Koch CJ. The relationship among hypoxia, proliferation, and outcome in patients with de novo glioblastoma: a pilot study. Transl Oncol. 2010;3(3):160–169.
4. Beppu T, Kamada K, Yoshida Y, Arai H, Ogasawara K, Ogawa A. Change of oxygen pressure in glioblastoma tissue under various conditions. J Neurooncol. 2002;58(1):47–52.
5. Evans SM, Judy KD, Dunphy I, Jenkins WT, Nelson PT, Collins R, Wileyto EP, Jenkins K, Hahn SM, Stevens CW, Judkins AR, Phillips P, Geoerger B, Koch CJ. Comparative measurements of hypoxia in human brain tumors using needle electrodes and EF5 binding. Cancer Res. 2004;64(5):1886–1892.
6. Bruehlmeier M, Roelcke U, Schubiger PA, Ametamey SM. Assessment of hypoxia and perfusion in human brain tumors using PET with 18F-fluoromisonidazole and 15O-H2O. J Nucl Med. 2004;45(11):1851–1859.
7. Spence AM, Muzi M, Swanson KR, O'Sullivan F, Rockhill JK, Rajendran JG, Adamsen TC, Link JM, Swanson PE, Yagle KJ, Rostomily RC, Silbergeld DL, Krohn KA. Regional hypoxia in glioblastoma multiforme quantified with [18F]fluoromisonidazole positron emission tomography before radiotherapy: correlation with time to progression and survival. Clin Cancer Res. 2008;14(9):2623–2630.
8. Cher LM, Murone C, Lawrentschuk N, Ramdave S, Papenfuss A, Hannah A, O'Keefe GJ, Sachinidis JI, Berlangieri SU, Fabinyi G, Scott AM. Correlation of hypoxic cell fraction and angiogenesis with glucose metabolic rate in gliomas using 18F-fluoromisonidazole, 18F-FDG PET, and immunohistochemical studies. J Nucl Med. 2006;47(3):410–418.
9. Swanson KR, Chakraborty G, Wang CH, Rockne R, Harpold HL, Muzi M, Adamsen TC, Krohn KA, Spence AM. Complementary but distinct roles for MRI and 18F-fluoromisonidazole PET in the assessment of human glioblastomas. J Nucl Med. 2009;50(1):36–44.
10. Cho H, Ackerstaff E, Carlin S, Lupu ME, Wang Y, Rizwan A, O'Donoghue J, Ling CC, Humm JL, Zanzonico PB, Koutcher JA. Noninvasive multimodality imaging of the tumor microenvironment: registered dynamic magnetic resonance imaging and positron emission tomography studies of a preclinical tumor model of tumor hypoxia. Neoplasia. 2009;11(3):247–259.
11. Thorwarth D, Eschmann SM, Scheiderbauer J, Paulsen F, Alber M. Kinetic analysis of dynamic 18F-fluoromisonidazole PET correlates with radiation treatment outcome in head-and-neck cancer. BMC Cancer. 2005;5:152.
12. Chabner BA, Bertino J, Cleary J, Ortiz T, Lane A, Supko JG, Ryan D. Cytotoxic agents. In: Brunton LL, Chabner BA, Knollmann BC, eds. Goodman & Gilman's The Pharmacological Basis of Therapeutics, 12th ed. New York, NY: The McGraw-Hill Companies; 2011.
13. Minchinton AI, Tannock IF. Drug penetration in solid tumours. Nat Rev Cancer. 2006;6(8):583–592.
14. Shannon AM, Bouchier-Hayes DJ, Condron CM, Toomey D. Tumour hypoxia, chemotherapeutic resistance and hypoxia-related therapies. Cancer Treat Rev. 2003;29(4):297–307.
15. Tatum JL, Kelloff GJ, Gillies RJ, Arbeit JM, Brown JM, Chao KS, Chapman JD, Eckelman WC, Fyles AW, Giaccia AJ, Hill RP, Koch CJ, Krishna MC, Krohn KA, Lewis JS, Mason RP, Melillo G, Padhani AR, Powis G, Rajendran JG, Reba R, Robinson SP, Semenza GL, Swartz HM, Vaupel P, Yang D, Croft B, Hoffman J, Liu G, Stone H, Sullivan D. Hypoxia: importance in tumor biology, noninvasive measurement by imaging, and value of its measurement in the management of cancer therapy. Int J Radiat Biol. 2006;82(10):699–757.
16. Del Rowe J, Scott C, Werner-Wasik M, Bahary JP, Curran WJ, Urtasun RC, Fisher B. Single-arm, open-label Phase II study of intravenously administered tirapazamine and radiation therapy for glioblastoma multiforme. J Clin Oncol. 2000;18(6):1254–1259.
17. Denny WA. Hypoxia-activated prodrugs in cancer therapy: progress to the clinic. Future Oncol. 2010;6(3):419–428.
18. Duan J-X, Jiao H, Kaizerman J, Stanton T, Evans JW, Lan L, Lorente G, Banica M, Jung D, Wang J, Ma H, Li X, Yang Z, Hoffman RM, Ammons WS, Hart CP, Matteucci M. Potent and highly selective hypoxia-activated achiral phosphoramidate mustards as anticancer drugs. J Med Chem. 2008;51(8):2412–2420.
19. Weiss GJ, Infante JR, Chiorean EG, Borad MJ, Bendell JC, Molina JR, Tibes R, Ramanathan RK, Lewandowski K, Jones SF, Lacouture ME, Langmuir VK, Lee H, Kroll S, Burris HA. Phase 1 study of the safety, tolerability, and pharmacokinetics of TH-302, a hypoxia-activated prodrug, in patients with advanced solid malignancies. Clin Cancer Res. 2011;17(9):2997–3004.
20. Hu J, Handisides DR, Van Valckenborgh E, De Raeve H, Menu E, Vande Broek I, Liu Q, Sun JD, Van Camp B, Hart CP, Vanderkerken K. Targeting the multiple myeloma hypoxic niche with TH-302, a hypoxia-activated prodrug. Blood. 2010;116(9):1524–1527.
21. Meng F, Evans JW, Bhupathi D, Banica M, Lan L, Lorente G, Duan JX, Cai X, Mowday AM, Guise CP, Maroz A, Anderson RF, Patterson AV, Stachelek GC, Glazer PM, Matteucci MD, Hart CP. Molecular and cellular pharmacology of the hypoxia-activated prodrug TH-302. Mol Cancer Ther. 2012;11(3):740–751.
22. Liu Q, Sun JD, Wang J, Ahluwalia D, Baker AF, Cranmer LD, Ferraro D, Wang Y, Duan JX, Ammons WS, Curd JG, Matteucci MD, Hart CP. TH-302, a hypoxia-activated prodrug with broad in vivo preclinical combination therapy efficacy: optimization of dosing regimens and schedules. Cancer Chemother Pharmacol. 2012;69(6):1487–1498.
23. Cardenas-Rodriguez J, Li Y, Galons JP, Cornnell H, Gillies RJ, Pagel MD, Baker AF. Imaging biomarkers to monitor response to the hypoxia-activated prodrug TH-302 in the MiaPaCa2 flank xenograft model. Magn Reson Imaging. 2012;30(7):1002–1009.
24. Sun JD, Liu Q, Wang J, Ahluwalia D, Ferraro D, Wang Y, Duan JX, Ammons WS, Curd JG, Matteucci MD, Hart CP. Selective tumor hypoxia targeting by hypoxia-activated prodrug TH-302 inhibits tumor growth in preclinical models of cancer. Clin Cancer Res. 2012;18(3):758–770.
25. Borad MJ, Reddy SG, Bahary N, Uronis HE, Sigal D, Cohn AL, Schelman WR, Stephenson J, Chiorean EG, Rosen PJ, Ulrich B, Dragovich T, Del Prete SA, Rarick M, Eng C, Kroll S, Ryan DP. Randomized Phase II trial of gemcitabine plus TH-302 versus gemcitabine in patients with advanced pancreatic cancer. J Clin Oncol. 2015;33(13):1475–1481.
26. Chawla SP, Cranmer LD, Van Tine BA, Reed DR, Okuno SH, Butrynski JE, Adkins DR, Hendifar AE, Kroll S, Ganjoo KN. Phase II study of the safety and antitumor activity of the hypoxia-activated prodrug TH-302 in combination with doxorubicin in patients with advanced soft tissue sarcoma. J Clin Oncol. 2014;32(29):3299–3306.
27. Valable S, Petit E, Roussel S, Marteau L, Toutain J, Divoux D, Sobrio F, Delamare J, Barre L, Bernaudin M. Complementary information from magnetic resonance imaging and (18)F-fluoromisonidazole positron emission tomography in the assessment of the response to an antiangiogenic treatment in a rat brain tumor model. Nucl Med Biol. 2011;38(6):781–793.
28. Valable S, Lemasson B, Farion R, Beaumont M, Segebarth C, Remy C, Barbier EL. Assessment of blood volume, vessel size, and the expression of angiogenic factors in two rat glioma models: a longitudinal in vivo and ex vivo study. NMR Biomed. 2008;21(10):1043–1056.
29. Khan N, Li H, Hou H, Lariviere JP, Gladstone DJ, Demidenko E, Swartz HM. Tissue pO2 of orthotopic 9L and C6 gliomas and tumor-specific response to radiotherapy and hyperoxygenation. Int J Radiat Oncol Biol Phys. 2009;73(3):878–885.

30. Valable S, Eddi D, Constans J-M, Guillamo J-S, Bernaudin M, Roussel S, Petit E. MRI assessment of hemodynamic effects of angiopoietin-2 overexpression in a brain tumor model. Neuro Oncol. 2009;11(5):488–502.

31. Tochon-Danguy HJ, Sachinidis JI, Chan F, Gordon Chan J, Hall C, Cher L, Stylli S, Hill J, Kaye A, Scott AM. Imaging and quantitation of the hypoxic cell fraction of viable tumor in an animal model of intracerebral high grade glioma using [18F]fluoromisonidazole (FMISO). Nucl Med Biol. 2002;29(2):191–197.

32. Mistry N, Stokes AM, Gambrell JV, Quarles CC. Nitrite induces the extravasation of iron oxide nanoparticles in hypoxic tumor tissue. NMR Biomed. 2014;27(4): 425–430.

33. Wang W, Lee NY, Georgi JC, Narayanan M, Guillem J, Schoder H, Humm JL. Pharmacokinetic analysis of hypoxia (18)F-fluoromisonidazole dynamic PET in head and neck cancer. J Nucl Med. 2010;51(1):37–45.

34. Wang K, Yorke E, Nehmeh SA, Humm JL, Ling CC. Modeling acute and chronic hypoxia using serial images of F18-FMISO PET. Med Phys. 2009;36(10):4400–4408.

35. Monnich D, Troost EG, Kaanders JH, Oyen WJ, Alber M, Thorwarth D. Modelling and simulation of the influence of acute and chronic hypoxia on [18F]fluoromisonidazole PET imaging. Phys Med Biol. 2012;57(6):1675–1684.

36. Wojtkowiak JW, Cornnell HC, Matsumoto S, Saito K, Takakusagi Y, Dutta P, Kim M, Zhang X, Leos R, Bailey KM, Martinez G, Lloyd MC, Weber C, Mitchell JB, Lynch RM, Baker AF, Gatenby RA, Rejniak KA, Hart C, Krishna MC, Gillies RJ. Pyruvate sensitizes pancreatic tumors to hypoxia-activated prodrug TH-302. Cancer Metab. 2015;3(1):2.

37. Takakusagi Y, Matsumoto S, Saito K, Matsuo M, Kishimoto S, Wojtkowiak JW, DeGraff W, Kesarwala AH, Choudhuri R, Devasahayam N, Subramanian S, Munasinghe JP, Gillies RJ, Mitchell JB, Hart CP, Krishna MC. Pyruvate induces transient tumor hypoxia by enhancing mitochondrial oxygen consumption and potentiates the anti-tumor effect of a hypoxia-activated prodrug TH-302. PloS One. 2014;9(9).

38. Krohn KA, Link JM, Mason RP. Molecular imaging of hypoxia. J Nucl Med. 2008;49(Suppl 2):129S–148S.

39. Dewhirst MW, Birer SR. Oxygen-Enhanced MRI is a major advance in tumor hypoxia imaging. Cancer Res. 2016;76(4):769–772.

40. O'Connor JP, Boult JK, Jamin Y, Babur M, Finegan KG, Williams KJ, Little RA, Jackson A, Parker GJ, Reynolds AR, Waterton JC, Robinson SP. Oxygen-Enhanced MRI accurately identifies, quantifies, and maps tumor hypoxia in preclinical cancer models. Cancer Res. 2016;76(4):787–795.

41. Hatano T, Zhao S, Zhao Y, Nishijima K, Kuno N, Hanzawa H, Sakamoto T, Tamaki N, Kuge Y. Biological characteristics of intratumoral [F-18]fluoromisonidazole distribution in a rodent model of glioma. Int J Oncol. 2013;42(3):823–830.